© MAY 2026 | IRE Journals | Volume 9 Issue 11 | ISSN: 2456-8880
DOI: https://doi.org/10.64388/IREV9I11-1717407

Analysing The Impact of Temperature Variation on The Performance Of 3-Phase Induction Motor for Industrial Applications

OGBU, OHEHA JOHN [1], GERTRUDE FISCHER [2], ASUQUO EKE[3]
[1,2,3] *Department of Electrical/Electronic Engineering Cross River University of Technology, Calabar. Nigeria*

Abstract- ***This study investigates the effects of asymmetrical thermal flow in three-phase induction motors, analyzing its impact on motor performance, efficiency, and longevity while proposing strategies for mitigation. The research aims to: Develop a computational model of a three-phase induction motor, simulate and analyze using ANSYS Motor-CAD 2025 R1.1, assess the impact of thermal asymmetry on motor performance and propose effective thermal management solutions. The study focuses on the thermal behavior of induction motors, particularly examining temperature distribution, heat dissipation, and efficiency losses due to asymmetrical thermal flow. It employs numerical simulations and analytical techniques to identify critical thermal zones and evaluate different cooling strategies. The research utilizes Finite Element Analysis (FEA) with ANSYS Motor-CAD 2025 R1.1 to model and simulate heat generation and dissipation in key motor components (stator, rotor, and windings). The simulations are conducted on a Dell Inspiron 5593 with an Intel Core i3-1005G1 CPU, ensuring accurate computational analysis. The study reveals that asymmetrical thermal flow leads to localized overheating, increasing winding resistance, reducing efficiency, and accelerating insulation degradation. Temperature variations of 74.7°C, 76.7°C, 88.7°C, and 86.5°C were recorded in different motor sections, with an acceptable thermal range of 10°C to 40°C. Optimized cooling mechanisms and material selection significantly reduce these effects, enhancing motor efficiency. The findings highlight the importance of effective thermal management in induction motors. Implementing optimized airflow, improved material selection, and enhanced cooling techniques can mitigate thermal imbalances, ensuring improved reliability and operational efficiency of induction motors in industrial application.***

Keyword: Induction motor, Temperature variation, Effect, industrial Applications

I. INTRODUCTION

The three-phase induction motor is the most widely used electrical machine in industrial, commercial, and domestic applications due to its robustness, reliability, simple design, and cost-effectiveness. It plays a critical role in driving mechanical loads across diverse sectors, from manufacturing plants to transportation systems. However, like all electromechanical devices, its performance is significantly influenced by operating conditions, with temperature variation being one of the most critical factors. Temperature rise in induction motors results from both electrical and mechanical losses, such as copper losses, core losses, stray load losses, and frictional losses, which are dissipated in the form of heat. If not properly managed, this thermal effect alters the machine's electrical, magnetic, and mechanical characteristics, ultimately affecting efficiency, reliability, and lifespan. Okoro (2003), A. Eke *et al* (2024). The performance of an induction motor is inherently tied to the temperature of its windings, stator core, and rotor. Elevated temperatures increase the resistance of stator and rotor windings, which leads to higher I^2R losses, reduced efficiency, and derating of output power. Furthermore, excessive heating accelerates insulation degradation, leading to reduced dielectric strength, shorter operational life, and potential catastrophic failure. Similarly, variations in cooling conditions or ambient temperature can influence the thermal balance of the motor, altering its torque speed characteristics and overall stability. On the other hand, operating the motor under very low temperatures may also affect lubrication, mechanical clearances, and magnetic properties of core materials, thereby impacting smooth operation. Okoro (2003), A. Eke *et al* (2024). Understanding the impact of

temperature variation is therefore crucial for optimal design, efficient operation, and effective thermal management of induction motors. It enables engineers to establish thermal models, predict performance limits, and implement proper protection mechanisms such as derating, thermal relays, and advanced cooling systems. Moreover, with the increasing demand for high-performance and energy-efficient machines, especially in traction, renewable energy, and industrial automation, comprehensive thermal analysis has become indispensable. This study aims to analyse how temperature variations affect key performance parameters such as efficiency, power factor, torque, speed, and lifespan of a three-phase induction motor, providing insights for improved design, control strategies, and preventive maintenance. Okoro (2003). The three-phase induction motor is the most widely utilized electrical machine in power systems and industrial applications due to its simplicity, ruggedness, low cost, and adaptability to a wide range of operating conditions. Its reliability and efficiency have made it the backbone of mechanical power conversion in sectors such as manufacturing, transportation, mining, and utilities. However, the performance of an induction motor is strongly influenced by temperature variations arising from internal heat generation and external ambient conditions. The heat in the machine is primarily produced by electrical losses (stator and rotor copper losses, core losses, stray losses) and mechanical losses (friction and windage). If not adequately managed, this thermal energy accumulates in the windings, rotor, and core, altering electrical, magnetic, and mechanical characteristics of the motor. From an electrical perspective, winding resistance is a key parameter influenced by temperature. The resistance of conductors varies approximately linearly with temperature. An increase in temperature leads to a rise in resistance, which in turn causes higher losses, reduces efficiency, and alters voltage drops across the stator and rotor circuits. The thermal effects extend to motor torque production as well. The electromagnetic torque of an induction motor. As temperature increases, R1 and R’2 increase, thereby modifying the torque slip characteristics and often reducing the maximum torque capability of the motor. The need for an accessible method of machine design arises from the fact that the motor is used for a variety of industrial applications. Analytical equations are typically used to dimension the magnetic and electric circuits in the basic design of an electrical machine. However, computer aided design is typically used to assess the machine's accurate performance. This computer-aided design (CAD) method allows for the efficient study of the impact of a single parameter on the machine's dynamical performance while utilizing a programming language. In order to perform the design calculations, this paper demonstrates a CAD approach (using Java), which simplified the design of a three-phase induction system. Purpose and Overview of The Research while developing a lumped parameter thermal model it was found that it is possible to develop a satisfactory thermal model using the dimensional details of the machine. The stator copper loss, rotor copper loss and iron loss are the input of the model and the temperature rise of different parts are the output. The detailed dimensional data are required to calculated the parameters of the thermal model. It was observed that the manufacturers are unwilling to supply the detailed dimensional data. What are available for a commercially designed machine the outer dimensions of the machine. The number of stator and rotor slots and their dimensions are difficult to obtain. In this work we have tried to develop the parameter of the thermal model from the outer dimensions of the machines.

II. METHODOLOGY

The d-q axis transformation theory of the stator and rotor variables in the arbitrary reference frame is applied in dynamic modelling of a three-phase asynchronous motor. This dynamic model describes the dynamic behavior of induction motor. It is known that the speed of rotation of the d-q axis can be arbitrary although there are three preferred speeds or referenced frames as follows (Sonakshi and Sulochana, 2014).

i. The stationary reference frame, where the d-q axis does not rotate.
ii. The rotor reference frame, where the d-q axis rotates at rotor speed
iii. The synchronous rotating reference frame, where the d-q axis rotates at synchronous speed

A generalized dynamic model of the induction motor consists of an electrical sub-model to implement the three-phase to two-axis transformation of the stator voltage and current calculation, a torque sub-model to calculate the develop electromagnetic torque and a mechanical sub-model to yield the rotor speed. In addition, a stator current output sub-model is needed for calculating the voltage drop in the supply cables.

2.1. DIRECT QUADRATURE (D-Q) TRANSFORMATION OF THREE PHASES INDUCTION MOTOR

In balanced three-phase circuit, application of the d-q transform reduces the three AC quantities to two DC quantities (Sonakshi and Sulochana, 2014).

The various stages applied to achieve d-q transformation are the Clarke's and the parks transformation.

2.2. THE CLARKE'S TRANSFORMATION

Clarkes explain as follows:
The three phase voltages varying in time along the axis a, b, and c, can be algebraically transformed into two voltages varying in time along the axis, α and β by the following transformation matrix in equation (1) (Sonakshi and Sulochana, 2014).

$$\begin{bmatrix} V_\alpha \\ V_\beta \end{bmatrix} = \frac{2}{3}\begin{bmatrix} 1 & -\frac{1}{2} & -\frac{1}{2} \\ 0 & \frac{\sqrt{3}}{2} & -\frac{\sqrt{3}}{2} \end{bmatrix}\begin{bmatrix} V_a \\ V_b \\ V_c \end{bmatrix} \quad (1)$$

Also, obtaining the three phase quantities from the two-phase quantities (inverse transformation) is possible through the transformation matrix in equation (2).

$$\begin{bmatrix} V_a \\ V_b \\ V_c \end{bmatrix} = \frac{2}{3}\begin{bmatrix} 1 & 0 \\ -\frac{1}{2} & \frac{\sqrt{3}}{2} \\ -\frac{1}{2} & \frac{\sqrt{3}}{2} \end{bmatrix}\begin{bmatrix} V_\alpha \\ V_\beta \end{bmatrix} \quad (2)$$

2.4. THE PARKS TRANSFORMATION

Parks explains as follows
The two-axis orthogonal stationary reference frame quantities are transformed into rotating reference frame quantities using the Parks transformation. The referred Parks transformation matrix is shown in equation (3).

$$\begin{bmatrix} V_d \\ V_q \end{bmatrix} = \begin{bmatrix} \cos\theta & \sin\theta \\ -\sin\theta & \cos\theta \end{bmatrix}\begin{bmatrix} V_\alpha \\ V_\beta \end{bmatrix} \quad (3)$$

Transforming the quantities from two-phase rotating to two-phase stationary frame can be achieved using the transformation matrix in equation (4) (Sonakshi and Sulochana, 2014), (eke et al 2025)

$$\begin{bmatrix} V_\alpha \\ V_\beta \end{bmatrix} = \begin{bmatrix} \cos\theta & -\sin\theta \\ \sin\theta & \cos\theta \end{bmatrix}\begin{bmatrix} V_d \\ V_q \end{bmatrix} \quad (4)$$

2.3. DYNAMIC MODEL EQUATION FOR THREE- PHASE INDUCTION MACHINE

The dynamic model equations of the induction motor can be obtained from the dq0 equivalent circuit of the induction motor shown in figure 1, figure 2, and figure 3. (TriptiRai and Prashant, 2016).(eke et al 2025)

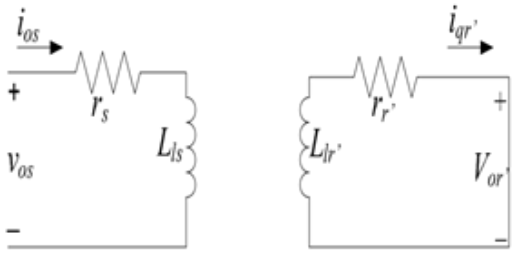

Fig. 1. Q-axis equivalent circuit of an induction motor.(eke et al 2026)

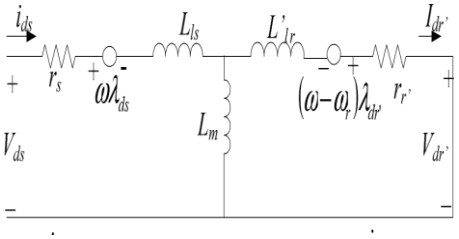

Fig. 2 D-axis equivalent circuit of an induction motor (eke et al 2026)

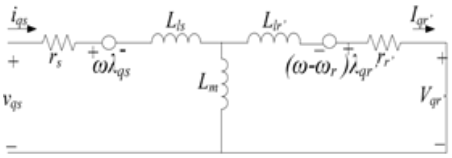

Fig. 3. Q-axis equivalent circuit of an induction motor(eke et al 2026)

© MAY 2026 | IRE Journals | Volume 9 Issue 11 | ISSN: 2456-8880
DOI: https://doi.org/10.64388/IREV9I11-1717407

Under balanced condition the three-phase stator voltage of an induction motor can be expressed as equation (5), (6), and (7).

$$Va = \sqrt{2}\,Vrms\,\sin(\omega t) \quad (5)$$

$$Vb = \sqrt{2}\,Vrms\,\sin\left(\omega t - \frac{2\pi}{3}\right) \quad (6)$$

$$Vc = \sqrt{2}\,Vrms\,\sin\left(\omega t + \frac{2\pi}{3}\right) \quad (7)$$

These three phase voltages are transformed into two phase synchronously rotating reference frame of dq0 axis. This transformation is achieved through the application of the following transformation matrix as shown in equation (8).

$$\begin{bmatrix} V_\alpha \\ V_\beta \end{bmatrix} = \frac{2}{3}\begin{bmatrix} 1 & \frac{1}{2} & -\frac{1}{2} \\ 0 & \frac{\sqrt{3}}{2} & -\frac{\sqrt{3}}{2} \end{bmatrix}\begin{bmatrix} V_a \\ V_b \\ V_c \end{bmatrix} \quad (8)$$

Then, the dq axis voltages are shown in equation (9):

$$\begin{bmatrix} V_d \\ V_q \end{bmatrix} = \begin{bmatrix} \cos\theta & \sin\theta \\ -\sin\theta & \cos\theta \end{bmatrix}\begin{bmatrix} V_\alpha \\ V_\beta \end{bmatrix} \quad (9)$$

The instantaneous value of the stator and rotor currents of a three-phase induction motor are calculated by using the following matrix equations (10) and (11); (eke et al 2026)

$$\begin{bmatrix} i_\alpha \\ i_\beta \end{bmatrix} = \begin{bmatrix} \cos\theta & -\sin\theta \\ \sin\theta & \cos\theta \end{bmatrix}\begin{bmatrix} i_d \\ i_q \end{bmatrix} \quad (10)$$

$$\begin{bmatrix} i_a \\ i_b \\ i_c \end{bmatrix} = \begin{bmatrix} 1 & 0 \\ \frac{1}{2} & -\frac{\sqrt{3}}{2} \\ -\frac{1}{2} & -\frac{\sqrt{3}}{2} \end{bmatrix}\begin{bmatrix} i_\alpha \\ i_\beta \end{bmatrix} \quad (11)$$

The stator and rotor voltage equation of the direct and quadrature (d-q) axis of an induction motor are given in equations (12), (13), (14), and (15).

$$V_{qs} = R_s\, i_{qs} + \frac{d}{dt}\lambda_{qs} + \omega_e \lambda_{qr} \quad (12)$$

$$V_{ds} = R_s i_{ds} + \frac{d}{dt}\lambda_{qs} - \omega_e\, \lambda_{ds} \quad (13)$$

$$V_{qr} = R_r i_{qr} + \frac{d}{dt}\lambda_{qr} + \left(\omega_e - \omega_r\right)\lambda_{qr} \quad (14)$$

$$V_{dr} = R_r i_{dr} + \frac{d}{dt}\lambda_{dr} - \left(\omega_e - \omega_r\right)\lambda_{dr} \quad (15)$$

Where, λ_{qr} , λ_{qs} , λ_{dr} , and λ_{ds} are the stator and rotor flux linkage of the d and q axis, these equations show the synchronously rotating reference frame for the two-phase d-q-axis of the induction motor.

For squirrel cage induction motor, the rotor voltages V_{qr}, V_{dr} are set to zero, since the rotor cage bars are shorted. Therefore, the flux linkage equation can be express as equations (16), (17), (18), (19), (20), (21), and (22).

$$\frac{d\lambda_{qs}}{dt} = \omega_b\left[V_{qs} - \frac{\omega_e}{\omega_b}\lambda_{ds} + \frac{R_s}{X_{ls}}\left(\lambda_{mq} - \lambda_{qs}\right)\right] \quad (16)$$

$$\frac{d\lambda_{ds}}{dt} = \omega_b\left[V_{ds} + \frac{\omega_e}{\omega_b}\lambda_{qs} + \frac{R_s}{X_{ls}}\left(\lambda_{md} - \lambda_{qs}\right)\right] \quad (17)$$

$$\frac{d\lambda_{qr}}{dt} = \omega_b\left[V_{qs} - \left(\frac{\omega_e - \omega_r}{\omega_b}\right)\lambda_{qr} + \frac{R_r}{X_{lr}}\left(\lambda_{mq} - \lambda_{qr}\right)\right] \quad (18)$$

$$\frac{d\lambda_{qr}}{dt} = \omega_b\left[V_{qs} + \left(\frac{\omega_e - \omega_r}{\omega_b}\right)\lambda_{qr} + \frac{R_r}{X_{lr}}\left(\lambda_{mq} - \lambda_{qr}\right)\right] \quad (19)$$

III. MATHEMATICAL MODEL: TEMPERATURE EFFECTS ON A 3-PHASE INDUCTION MOTOR

The following assumptions are considered

Balanced three-phase supply, sinusoidal.

Squirrel-cage induction motor, parameters referred to stator.

Temperature is spatially lumped: single winding/core temperature Tw(t)

Material coefficients (e.g., α\alphaα of copper) constant over operating range.

Cooling described by convective heat transfer to ambient. (eke et al 2025), (eke et al 2025)

3.1 ELECTRICAL MODEL (STEADY STATE, PER-PHASE EQUIVALENT REFERRED TO STATOR)

Per-phase equivalent circuit parameters:

$R_1(T)$ stator resistance at temperature T.

X_1 stator leakage reactance (weakly dependent on T; often treated constant).

$R'_2(T)$ rotor resistance referred to stator at temperature T.

X'_2 rotor leakage reactance (treated constant or weak temp dependence).

V_1 phase voltage magnitude.

s slip ($0 < s \leq 1$).

For temperature dependence of resistances

$$R(T) = R_{ref}\backslash big\left[1 + \alpha\left(T - T_{ref}\right)\backslash big\right] \quad (20)$$

where α is temperature coefficient

thus,

$$R_1(T) = R_{1,ref}\left[1 + \alpha(T - T_{ref})\right], \quad R_2'(T) = R_{2,ref}'\left[1 + \alpha(T - T_{ref})\right] \tag{21}$$

Per-phase current

$$I_1 = \frac{V_1}{Z_{eq}} \quad \text{with} \quad Z_{eq} = R_1(T) + jX_1 + \frac{\left(jX_2' + R_2'(T)/s\right) \cdot 0}{(\text{use full derivation})}. \tag{22}$$

Air-gap power (per phase) and electromagnetic torque

Total air-gap power (three-phase):

$$P_{ag} = 3 \cdot I_2'^2 \cdot \frac{R_2'(T)}{s} \tag{23}$$

Electromagnetic torque: (eke et al 2025)

$$T_e = \frac{P_{ag}}{\omega_s} = \frac{3\, I_2'^2\, R_2'(T)}{s\, \omega_s} \tag{24}$$

using classical torque-slip closed form

$$T_e(s,T) = \frac{3V_1^2 (\backslash dfrac R_2'(T) s)}{\omega_s \left[(R_1(T) + \backslash dfrac R_2'(T) s)^2 + (X_1 + X_2')^2\right]} \tag{25}$$

LOSS MODEL

Copper losses (stator + rotor)

$$P_{cu1} = 3I_1^2 R_1(T), \qquad P_{cu2} = 3I_2'^2 R_2'(T) \tag{26}$$

Often approximate as

$$P_{fe} = k_h f B_{max}^2 + k_e f^2 B_{max}^2 \tag{27}$$

MECHANICAL (friction & windage)

$$P_{mec} = k_{fw}\, \omega_m^2 \tag{28}$$

tray losses

Aggregate other losses; may be modelled as a fraction of load or via empirical function $P_{stray}(T,\omega)$

Input power and efficiency

$$P_{in} = 3V_1 I_1 \cos \tag{29}$$

$$P_{out} = T_e \omega_m - P_{mec} \tag{30}$$

$$\eta = \frac{P_{out}}{P_{in}} = \frac{P_{in} - (P_{cu1} + P_{cu2} + P_{fe} + P_{mec} + P_{stray})}{P_{in}} \tag{31}$$

THERMAL MODEL (lumped-parameter, first-order RC)

Heat balance (lumped)

$$C_{th} \frac{dT(t)}{dt} = P_{loss}(t) - H(T(t) - T_{amb}) \tag{32}$$

where:

T(t) winding/core temperature (°C).

T_{amb} ambient temperature.

C_{th} thermal capacitance (J/°C).

H overall heat transfer coefficient (W/°C) representing convection + conduction to ambient.

$$P_{loss}(t) = P_{cu1} + P_{cu2} + P_{fe} + P_{stray} + P_{mec} \tag{33}$$

THERMAL TIME CONSTANT

$$\tau_{th} = \frac{C_{th}}{H} \tag{34}$$

At steady-state:

$$T_{ss} = T_{amb} + \frac{P_{loss,ss}}{H} \tag{35}$$

Insulation ageing (lifetime model)

Arrhenius relation (absolute temperature)

$$L(T) = L_0 \exp !\backslash Big\left(-\frac{E_a}{k_B (T + 273.15)}\backslash Big\right) \tag{36}$$

Life halves for each $\Delta T \approx 10^{\circ C}$ (empirical)

The simulation is done in three stages of temperature rage as shown in the table 1

Table 1: Temperature variations

MOTOR PARTS	Normal Temperature	Temperature Test 1	Temperature Test 2
Armature winding Temperature	40	120	180
Bar Temperature	140	180	280
End Ring Temperature	140	180	280
Shaft temperature	40	70	100
Air gap Temperature	20	20	20
Rotor /Stator Laminatio	20	20	20

© MAY 2026 | IRE Journals | Volume 9 Issue 11 | ISSN: 2456-8880
DOI: https://doi.org/10.64388/IREV9I11-1717407

n Temperature			
Bearing Temperature	20	20	20

IV. RESULTS PRESENTATION

The result gotten uses the values in table 1

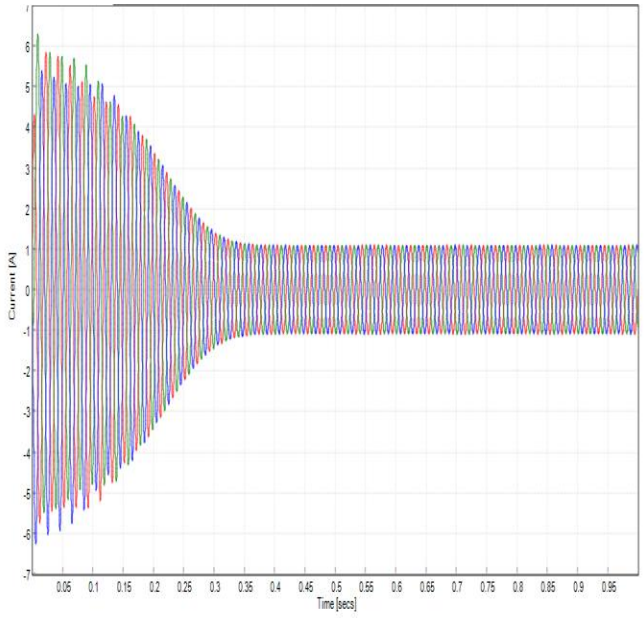

Fig. 4: Graph of Current against time

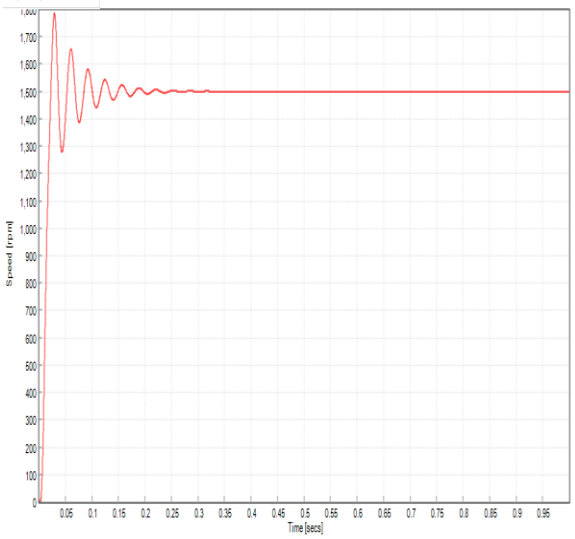

Fig. 5: graph of Speed against time

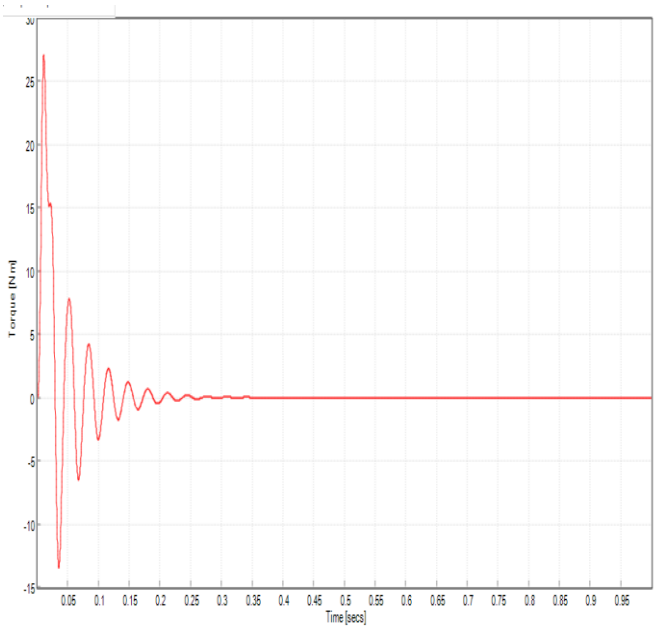

Fig. 6: Graph of Torque against time

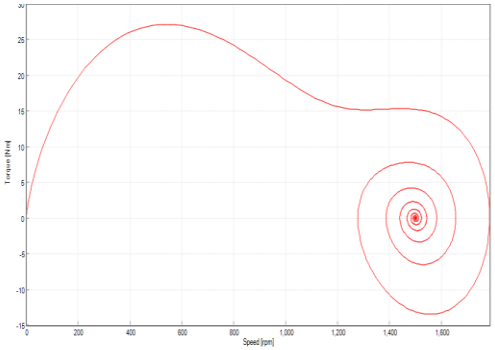

Fig. 7: Graph of Torque against speed

© MAY 2026 | IRE Journals | Volume 9 Issue 11 | ISSN: 2456-8880
DOI: https://doi.org/10.64388/IREV9I11-1717407

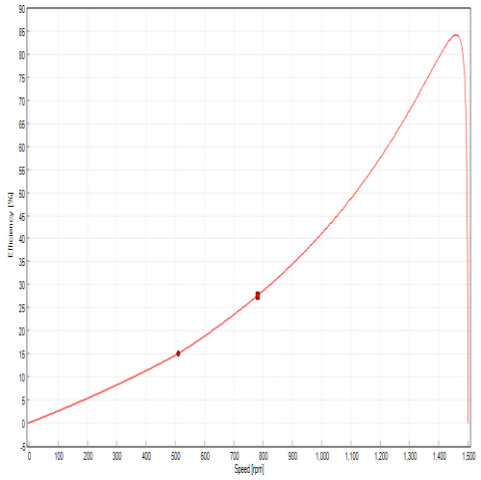

Fig. 8: Graph of Efficiency against Speed

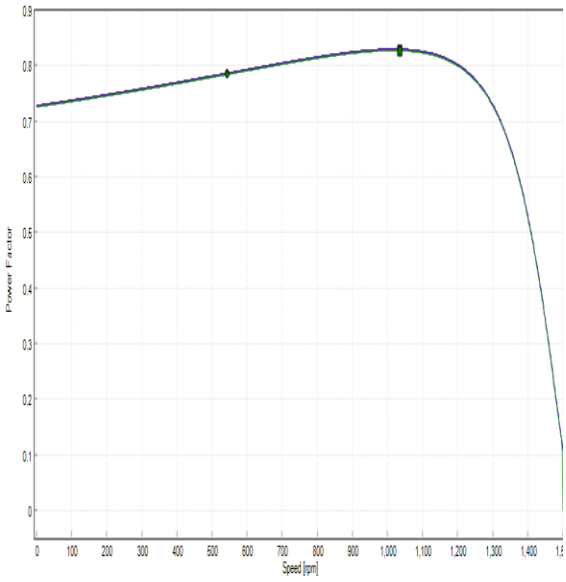

Fig. 9: Graph of Power factor against Speed

4.2 RESRESULTS DISCUSSION

Fig. 4 Graph of Current against Time, the figure shows the three-phase stator currents (sinusoidal waveforms, phase-shifted by 120°). At the start (t = 0), the motor draws a very high inrush current (several times the rated current). This is typical because at standstill the rotor slip s≈1s, rotor EMF is maximum, and the rotor resistance is very small compared to reactance. The oscillations gradually decrease in amplitude as the motor accelerates and approaches steady-state speed. After ~0.3s, the currents settle to a nearly constant sinusoidal magnitude, representing steady-state balanced operation. Physically, this demonstrates the transient-to-steady state behaviour of stator currents during motor starting. With higher temperature, stator resistance Rs increases. This leads to higher copper losses (I^2R) and faster damping of current oscillations. The peak inrush current may slightly reduce (due to higher resistance), but overall efficiency drops. Long-term steady-state current will be higher for the same load, since more current is needed to overcome resistive losses. Fig. 5 Graph of Speed against Time, the rotor speed starts from zero at t = 0. It rises sharply during the transient, experiencing small oscillations (speed ripple) due to torque pulsations during acceleration. Eventually, the speed settles to a steady-state close to synchronous speed (around 1500 rpm for a 4-pole, 50 Hz machine). The small gap between synchronous speed and the final steady-state speed represents the slip, which is necessary for torque production. This figure shows how quickly the motor accelerates and how effectively it damps oscillations before reaching steady-state operation. slower acceleration, meaning the curve would take longer to settle at steady-state. The final steady-state speed would also be slightly lower, because higher slip is required to produce the same load torque. In summary: temperature rise shifts the curve downward and rightward (lower speed, longer acceleration. Fig. 6: Graph of Torque against Time, at startup, the torque exhibits a high oscillatory transient response, swinging between positive and negative values. This corresponds to the motor's electromagnetic torque trying to overcome inertia and load torque. The oscillations reduce with time as damping increases, and the torque settles around a steady-state value slightly above zero (enough to counteract load torque and mechanical losses). The initial overshoot and oscillations are typical of transient electromagnetic torque due to sudden energization of the motor. Physically, this shows how the machine transitions from dynamic acceleration torque to steady-state running torque. With hotter windings, the torque oscillations would be smaller in amplitude because of higher electrical damping. However, the steady-state torque decreases, since torque is inversely related to rotor resistance at low

slip. Startup torque in particular is most affected: at high resistance, the maximum starting torque reduces, possibly making it harder to drive heavy loads. Fig. 7 Graph of Torque against Speed, this is the torque–speed characteristic, plotted dynamically during startup. Starting from zero speed, the torque rises steeply, reaches a maximum torque (pull-out torque) around mid-slip (~0.2–0.3 Pu slip), and then decreases as the motor approaches synchronous speed. The spiral shape in the plot results from the dynamic path of the motor: as speed increases and torque oscillates, the trajectory spirals inward before stabilizing at the steady-state operating point. This figure clearly illustrates the nonlinear relationship between torque and speed in induction motors: high torque at intermediate slips, decreasing torque as slip approaches zero. The final point of the spiral corresponds to the steady-state speed where the developed torque equals the load torque. The torque–speed characteristic shifts downward as resistance increases. The pull-out torque (maximum torque) decreases, and it occurs at a higher slip. This means the motor must run at a higher slip (lower speed) to maintain the same torque when hot. The spiral trajectory in the figure would become wider and settle at a lower speed operating point. Fig. 8 Efficiency vs Speed, at low speeds (left side of the curve), the efficiency is very low. This is because copper losses (I^2R) and core losses dominate, while the output power is still small. The motor is consuming energy but not yet converting much of it into useful mechanical output. As the speed increases toward synchronous speed, efficiency improves steadily. This happens because the output mechanical power increases faster than the losses. The efficiency peaks close to rated operating speed (around 1450 rpm for a 4-pole, 50 Hz motor). This is the normal operating point where the induction motor is designed to run with maximum efficiency. After the peak, efficiency drops sharply as the motor approaches synchronous speed. At this point, the slip becomes extremely small, torque falls, and mechanical output reduces, while losses (such as iron losses and stray load losses) remain. If temperature increases, winding resistance rises, leading to higher copper losses. This would lower the efficiency curve at all speeds and shift the peak efficiency slightly downward. Fig. 9: Power Factor vs Speed, at very low speeds (high slip), the power factor is poor (low value). This is because the motor draws a large magnetizing current and reactive component to establish the air-gap flux, while real power (torque production) is small. As the motor accelerates, the power factor increases gradually. Around mid-to-high speeds, the power factor reaches a maximum, typically close to rated speed. Here, the motor draws proportionally more real power compared to reactive power, which is favourable for the supply system. Near synchronous speed, the power factor drops again sharply. This is because the slip is very small, rotor current reduces significantly, and the motor draws mostly magnetizing (reactive) current with little real power transfer. The graph shows this classic "rise–peak–fall" profile of induction motor power factor. Higher temperatures increase resistance, which slightly reduces the power factor (since more current is wasted as resistive losses rather than useful torque). The maximum power factor point would be lower in magnitude compared to a cooler motor.

Table 2: summary of the motor performance with temperature variations

Motor Performance	Normal Temperature	Temperature Test I	Temperature Test II
Starting current (A)	6.5	22.5	14
Speed (rpm)	1800	1700	1600
Torque (Nm)	27.5	26	23
Efficiency (%)	85	70	65
Power Factor	0.80	0.75	0.70
Output Power (W)	2000	1518	1395.5

Table 2 presents the performance characteristics of a three-phase induction motor under three different operating conditions: Normal Temperature, Temperature Test I, and Temperature Test II. Each row describes a key performance parameter of the motor and shows how it is influenced by increasing temperature. The table clearly shows that increasing temperature has a negative impact on motor performance. Starting current increases sharply,

stressing the motor windings. Speed and torque reduce, lowering the motor's ability to drive loads effectively. Efficiency and power factor fall, leading to higher losses and poorer energy utilization. Output power declines, reducing the motor's usable capacity. This implies that thermal effects are critical in motor design and operation, and proper cooling systems are essential to maintain efficiency, reliability, and lifespan.

V. CONCLUSION

This study demonstrates that temperature variation has a pronounced and multifaceted impact on the performance of three-phase squirrel-cage induction motors: rising winding and rotor temperatures increase conductor resistance, which elevates copper losses, reduces efficiency, lowers starting and maximum torque, increases steady-state slip (thus reducing operating speed under load), and accelerates insulation ageing thereby shortening service life and raising failure risk; conversely, very low temperatures can impair lubrication and magnetic properties. Coupled electro-thermal modelling and simulation confirm the feedback loop between losses and temperature (thermal runaway risk under poor cooling), and indicate that performance metrics such as current transients, torque speed curves, efficiency, and power factor all degrade measurably as operating temperature departs from nominal conditions. These results underscore that thermal behavior is a first-order design and operational constraint for reliable, efficient motor operation. Rising temperature generally increases starting current, leading to overheating risks and reduced motor life. Higher temperatures reduce torque-producing capability, increase slip, and slow down the motor. Heating reduces electromagnetic torque due to increased copper losses, decreased flux, and weakened magnetic field. At higher temperatures, copper and iron losses increase, lowering efficiency. Worsening power factor indicates higher reactive power demand as motor performance degrades with heating. As motor temperature increases, mechanical output power decreases due to reduced torque, efficiency, and speed.

REFERENCES

[1] Adebayo, I. A., & Akinlabi, S. A. (2011). Performance analysis of induction motors under varying load conditions. *International Journal of Engineering Research & Technology, 4*(3), 100-105.

[2] Adebayo, S. O., Olawale, I., & Adekunle, T. (2021). Energy-efficient induction motors in Nigerian industries: Challenges and opportunities. African Journal of Energy Research, 15(2), 45-60.

[3] Adefemi, J. O., Ajibade, S. A., & Kayode, T. (2021). Analysis of thermal stresses in three-phase induction motors in Nigerian industries. Journal of Applied Engineering Research, 18(3), 105-118.

[4] Adouni, A., & Marques Cardoso, J. (2021). Thermal analysis of low-power three-phase induction motors operating under voltage unbalance and inter-turn short circuit faults. Machines, 9(1), 2. https://dx.doi.org/10.3390/machines9010002

[5] Afrah Thamer Abdullah, & Dr. Amer Mejbel Ali. (2019). Thermal analysis of a three-phase induction motor based on motor-CAD, flux2D, and MATLAB. Indonesian Journal of Electrical Engineering and Computer Science, 15(1), 46-53.

[6] Ahmed, F.; Roy, P.; Towhidi, M.; Feng, G.; Kar, N.C. CFD and LPTN Hybrid Technique to Determine Convection Coefficient in End-winding of TEFC IM with Copper Rotor. In Proceedings of the IECON 2019-45th Annual Conference of the IEEE Industrial Electronics Society, Lisbon, Portugal, 14–17 October 2019; IEEE: New York, NY, USA; Volume 1, pp. 939–944.

[7] Ali, J.A.; Hannan, M.A.; Mohamed, A.; Hussain, A. Optimization techniques to enhance the performance of IM drives: A review. Renew. Sustain. Energy Rev. 2018, 81, 1611–1626. [CrossRef]

[8] Arumugam, R.; Srinivas, K.N. Analysis and characterization of switched reluctance motors: Part II. Flow, thermal, and vibration analyses.

IEEE Trans. Magn. 2005, 41, 1321–1332. [CrossRef]

[9] Asuquo Eke, Fischer, G., David, A., Ekpenyong, O., & EJ, A. (2024). The Effect Of Rotor and Stator Slot Numbers On The Performance Of Three-Phase Induction Motors Used for Transport Application. IOSR Journal of Electrical and Electronics Engineering (IOSR-JEEE), Volume 19, Issue 4 Ser. 1 (July. – August. 2024), PP 01-09

[10] Asuquo Eke, Akpama E. J., Archibong E., Akisot E. (2021). Performance, Evaluation of Three Phase Induction Machine Control Using Simulink. International Journal of Innovative Science, Engineering & Technology, Volume 8, Issue 9, Pages 261 – 267, Publisher IJISET

[11] Aydin, I., Yildiz, M., & Güler, A. (2020). Analysis of thermal stress in induction motors under unbalanced load conditions. IEEE Transactions on Industrial Electronics, 67(6), 1234-1241.

[12] Aydin, M., Huang, S., & Lipo, T. A. (2020). Thermal analysis and modeling of induction motors under unbalanced conditions. IEEE Transactions on Energy Conversion, 35(2), 1053–1061.

[13] Benjamin, A. (2014). Fundamentals of electrical machines (2nd ed.). McGraw-Hill.

[14] Bianchi, N., Bolognani, S., & Dai Prè, M. (2005). Thermal analysis of induction and synchronous reluctance motors. IEEE Transactions on Industry Applications, 41(6), 1667–1675.

[15] Boglietti, A.; Cavagnino, A.; Staton, D.; Shanel, M.; Mueller, M.; Mejuto, C. Evolution and modern approaches for thermal analysis of electrical machines. IEEE Trans. Ind. Electron. 2009, 56, 871–882. [CrossRef]

[16] Boglietti, A.; Nategh, S.; Carpaneto, E.; Boscaglia, L.; Scema, C. An optimization method for cooling system design of traction motors. In Proceedings of the 2019 IEEE International Electric Machines & Drives Conference (IEMDC), San Diego, CA, USA, 12–15 May 2019; IEEE: New York, NY, USA; pp. 1210–1215.

[17] Bonnett, A. H., & Soukup, G. C. (1992). Cause and analysis of stator and rotor failures in three-phase squirrel-cage induction motors. IEEE Transactions on Industry Applications, 28(4), 921–937. https://doi.org/10.1109/28.150928

[18] Brown, J., & Davis, M. (1995). Thermal effects in inverter-fed induction motors. IEEE Transactions on Industry Applications, 31(6), 1283–1292.

[19] Brown, J., Smith, K., & Wang, T. (1978). Localized heating effects in induction motor rotors. IEEE Transactions on Energy Conversion, 12(4), 567–572.

[20] Cavagnino, A.; Boglietti, A.; Staton, D.; Shanel, M.; Mueller, M.; Mejuto, C. Evolution and modern approaches for thermal analysis of electrical machines. IEEE Trans. Ind. Electron. 2009, 56, 871–882. [CrossRef]

[21] Chapman, S. J. (2012). Electric machinery fundamentals (5th ed.). McGraw-Hill.

[22] Chen, L., Wang, H., & Zhang, Y. (2019). CFD analysis of thermal performance in electric machines. Applied Thermal Engineering, 161, 114039.

[23] Chen, X., Li, Y., & Zhang, M. (2021). Historical perspectives on induction motor design and challenges. IEEE Transactions on Industrial Applications, 57(3), 1234-1245.

[24] Chen, Z., Wang, H., & Liu, J. (2018). Impact of thermal gradients on core losses in induction motors: A theoretical and experimental study. Journal of Electrical Engineering, 25(4), 451-461.

[25] Chen, Z., Wang, H., & Liu, J. (2019). Thermal performance improvement in electric vehicle motors using advanced cooling strategies. Journal of Electric Machines, 27(4), 341-358.

[26] Eke, A., Okoro, O.I. and Onah, A.J., (2026). Multi-Objective Design and Optimization of a Three-Phase Induction Motor for Traction Application. IOSR Journal of Electronics and Communication Engineering (IOSR-JECE). Volume 21, Issue 2, Ser. 1 (Mar – Apr 2026), PP 29-37, 2026

[27] Asuquo Eke, O. I. Okoro, A. J. Onah. (2025). The Impact Of Changing Magnetization

Reactance Value On The Performance Of Three-Phase Induction Motor. Journal of Electrical and Electronics Engineering (IOSR-JEEE) e-ISSN: 2278-1676, p-ISSN: 2320-3331, Volume 20, Issue 6 Ser. 1 (Nov. – Dec. 2025), PP 01-08

[28] Asuquo Eke, O. I. Okoro, A. J. Onah, E. J. Akpama. (2025). Design And Thermal Modelling Of Induction Motor ForProlong Lifespan, IOSR Journal of Electronics and Communication Engineering (IOSR-JECE)e-ISSN: 2278-2834, p- ISSN: 2278-8735.Volume 20, Issue 6, Ser. I (Nov – Dec 2025), PP 81-89 *(PDF) Design And Thermal Modelling Of Induction Motor For Prolong Lifespan*. Available from: https://www.researchgate.net/publication/398860580_Design_And_Thermal_Modelling_Of_Induction_Motor_For_Prolong_Lifespan [accessed May 04 2026].